

Field-induced Néel vector bi-reorientation of a ferrimagnetic insulator in the vicinity of compensation temperature

Peng Wang(王鹏), Hui Zhao(赵辉), Zhongzhi Luan(栾仲智), Siyu Xia(夏思宇), Tao Feng(丰韬), and Lifan Zhou(周礼繁)

Citation: Chin. Phys. B, 2021, 30 (**2**): 027501. DOI: 10.1088/1674-1056/abbbef
Journal homepage: http://cpb.iphy.ac.cn; http://iopscience.iop.org/cpb

What follows is a list of articles you may be interested in

Magnetization reorientation induced by spin–orbit torque in YIG/Pt bilayers

Ying-Yi Tian(田颖异), Shuan-Hu Wang(王拴虎), Gang Li(李刚), Hao Li(李豪), Shu-Qin Li(李书琴), Yang Zhao(赵阳), Xiao-Min Cui(崔晓敏), Jian-Yuan Wang(王建元), Lv-Kuan Zou(邹吕宽), and Ke-Xin Jin(金克新)

Chin. Phys. B, 2020, 29 (**11**): 117504. DOI: 10.1088/1674-1056/abb666

Magnetism manipulation in ferromagnetic/ferroelectric heterostructures by electric field induced strain

Xiaobin Guo(郭晓斌), Dong Li(李栋), Li Xi(席力)

Chin. Phys. B, 2018, 27 (**9**): 097506. DOI: 10.1088/1674-1056/27/9/097506

Voltage control of magnetization switching and dynamics

Hong-Yu Wen(文宏玉), Jian-Bai Xia(夏建白)

Chin. Phys. B, 2018, 27 (**6**): 067502. DOI: 10.1088/1674-1056/27/6/067502

First-order reversal curve investigated magnetization switching in Pd/Co/Pd wedge film

Yan Li(李岩), Wei He(何为), Rui Sun(孙瑞), Zi-Zhao Gong(弓子召), Na Li(李娜), Qeemat Gul, Xiang-Qun Zhang(张向群), Zhao-Hua Cheng(成昭华)

Chin. Phys. B, 2018, 27 (**4**): 047503. DOI: 10.1088/1674-1056/27/4/047503

Control of spins in a nano-sized magnet using electric-current

Hong-yu Wen(文宏玉), Jian-bai Xia(夏建白)

Chin. Phys. B, 2017, 26 (**4**): 047501. DOI: 10.1088/1674-1056/26/4/047501

Field-induced Néel vector bi-reorientation of a ferrimagnetic insulator in the vicinity of compensation temperature*

Peng Wang(王鹏)[1,†], Hui Zhao(赵辉)[2], Zhongzhi Luan(栾仲智)[2], Siyu Xia(夏思宇)[2], Tao Feng(丰韬)[2], and Lifan Zhou(周礼繁)[2,‡]

[1] College of Mathematics and Physics, Qingdao University of Science and Technology, Qingdao 266061, China
[2] National Laboratory of Solid State Microstructures, Jiangsu Provincial Key Laboratory for Nanotechnology and Department of Physics, Nanjing University, Nanjing 210093, China

(Received 25 July 2020; revised manuscript received 5 September 2020; accepted manuscript online 28 September 2020)

The spin Hall magnetoresistance (SMR) effect in Pt/$Gd_3Fe_5O_{12}$ (GdIG) bilayers was systematically investigated. The sign of SMR changes twice with increasing magnetic field in the vicinity of the magnetization compensation point (T_M) of GdIG. However, conventional SMR theory predicts the invariant SMR sign in the heterostructure composed of a heavy metal film in contact with a ferromagnetic or antiferromagnetic film. We conclude that this is because of the significant enhancement of the magnetic moment of the Gd sub-lattice and the unchanged moment of the Fe sub-lattice with a relatively large field, meaning that a small net magnetic moment is induced at T_M. As a result, the Néel vector aligns with the field after the spin-flop transition, meaning that a bi-reorientation of the Néel vector is produced. Theoretical calculations based on the Néel's theory and SMR theory also support our conclusions. Our findings indicate that the Néel-vector direction of a ferrimagnet can be tuned across a wide range by a relatively low external field around T_M.

Keywords: spin Hall magnetoresistance, ferrimagnets, magnetic insulators, magnetization switching

PACS: 75.47.–m, 75.50.Gg, 75.60.Jk **DOI:** 10.1088/1674-1056/abbbef

1. Introduction

In ferrimagnetic materials, the magnetic moments in two or more magnetic sub-lattices with different magnetic moments are anti-ferromagnetically exchange-coupled, resulting in non-zero magnetic moments and angular momenta at absolute zero temperature. If the sub-lattice with a higher magnetic moment has a weaker molecular field than that of the sub-lattice with a lower magnetic moment, the total magnetization and angular momentum can be zero at certain temperatures, called the magnetization compensation point (T_M) and the angular momentum compensation point (T_A), respectively, owing to the different rates of decrease with temperature for diverse sub-lattices. Recently, the physical properties in the vicinity of T_M and T_A have received increasing attention for their rich physics and potential high-speed and low-energy-consumption spintronic applications.[1] For instance, the size of the skyrmions is reducible to the dimension of 10 nm in the vicinity of T_M because of the significantly weak stray field.[2] The spin–orbit-torque efficiency substantially increases close to T_M due to the negative exchange interaction in ferrimagnets.[3,4] The domain wall motion mobility was found to be enhanced dramatically up to 2×10^4 m·s^{-1}·T^{-1} close to T_A in GdFeCo.[5]

In anti-ferromagnetic (AFM) spintronics, the control of the Néel vector is of vital importance as it forms the basis for AFM information devices.[6] Two methods of manipulating the Néel vector have been widely investigated: electric current and magnetic field (H). The Néel-order manipulation by current was first reported in the conducting AFM CuMnAs via the staggered current-induced effective field.[7] Recent works have claimed the current-induced switching of the Néel vector via the spin–orbit torque from an adjacent heavy metal layer,[8,9] but the validity of the experimental evidence is still under debate.[10] The Néel vectors of anti-ferromagnets can be switched to perpendicular to H above a critical field,[11] known as the spin-flop (SF) transition. The AFM SF is widely used in the studies of spin transport in AFM insulators such as the spin Seebeck effect,[12] AFM magnon transport,[13] and spin superfluidity.[14,15] A field of the order of 10 T is usually required to achieve the SF phase.[16,17] The sub-lattice moments can be canted and then tuned to be aligned parallel to each other with a further increase in H. Ferrimagnets can be regarded as quasi-antiferromagnets in terms of nearly zero total moments in the vicinity of T_M. In comparison with anti-ferromagnets, the compensated ferrimagnets show richer magnetic order transitions close to T_M and their Néel vector

*Project supported by the National Key Research and Development Program of China (Grant Nos. 2017YFA0303202 and 2016YFA0300803), the National Natural Science Foundation of China (Grant Nos. 11904194, 11727808, and 11674159), and the Fundamental Research Funds for the Central Universities, China (Grant No. 020414380121).

†Corresponding author. E-mail: pwang7000@163.com
‡Corresponding author. E-mail: lifan-zhou@foxmail.com

© 2021 Chinese Physical Society and IOP Publishing Ltd

is easier to manipulate,[18–20] providing another platform for studying the rich physics related to the Néel order. However, at present, it is generally believed that the Néel vector of the compensated ferrimagnets undergoes an SF transition, and then all the sub-lattice moments turn toward H with a further increase in H.[18,19,21]

Most of the magnetic measurement techniques are not able to measure the Néel vector of the compensated ferrimagnets because of the near-zero magnetization. The spin Hall magnetoresistance (SMR)[22,23] was previously demonstrated to act as a convenient tool for measuring the orientation of the Néel vector of an AFM insulator.[24–26] In this study, we successfully used SMR to assess the magnetic order transition induced by the temperature (T) and H around T_M of $Gd_3Fe_5O_{12}$ (GdIG). Notably, the SMR is negative sign for a certain range of H around T_M. In contrast, the SMR is always positive for temperatures far from T_M. We attributed this to the switching of the Néel-vector direction of GdIG twice by H around T_M, meaning that bi-orientation of the GdIG Néel vector is achieved. The theoretical calculations combining the Néel's theory[27] and SMR theory[25,28] of ferrimagnetism are consistent with our observations and demonstrate the bi-reorientation of the Néel vector.

2. Experimental details

Single-crystalline GdIG films were epitaxially grown on $Gd_3Ga_5O_{12}$ (111) (GGG) substrates by pulsed laser deposition (PLD) at 750 °C. The oxygen pressure during deposition was 9×10^{-3} Torr (1 Torr = 1.33322×10^2 Pa) and the background vacuum was 2×10^{-7} Torr. The energy of the laser pulse was 230 mJ/mm^2. The surface morphology of the GdIG films was characterized by atomic force microscopy (AFM). The results are shown in Fig. 1(a). The film is significantly smooth with a root-mean-square (RMS) roughness of 0.227 nm over a scanning area of 2 μm×2 μm. Figure 1(b) shows the x-ray diffraction (XRD) pattern of the GdIG/GGG film. A strong GdIG (444) peak was observed, indicating a good crystal quality. The magnetic properties of GdIG were characterized by a quantum design superconducting quantum interference device vibrating sample magnetometer (SQUID-VSM). The Pt Hall bars with 0.3-mm wide and 3-mm long were deposited on the GdIG films through a shadow mask by direct current (DC) magnetron sputtering at room temperature. The magnetoresistance (MR) measurements were performed in a physical property measurement system (PPMS) using the four-wire method with a combination of a Keithley 2400 SourceMeter and a Keithley 2002 voltmeter.

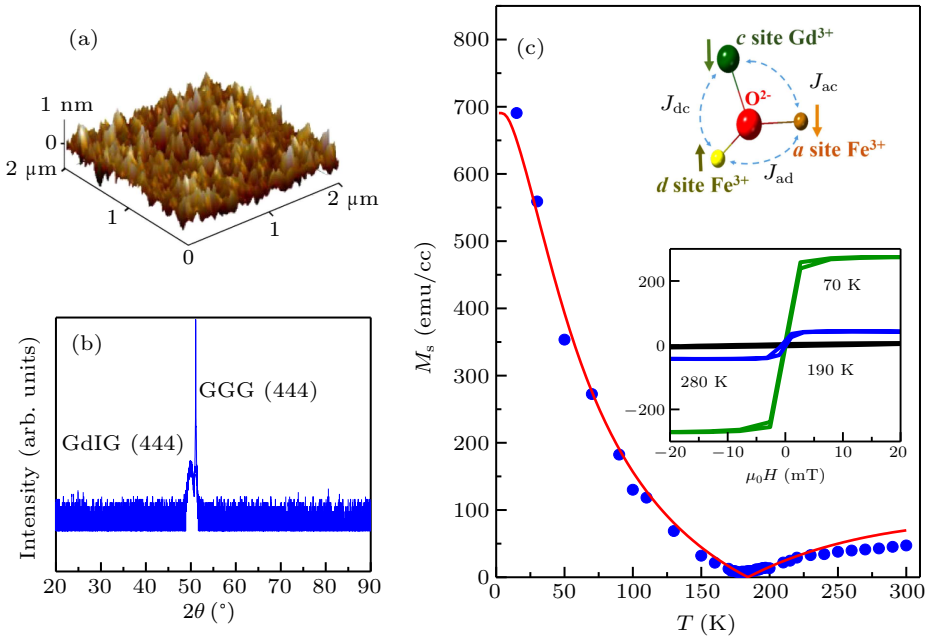


Fig. 1. (a) AFM topography image of the GdIG/GGG (111) film. Root-mean-square roughness is 0.272 nm. (b) XRD pattern of our GdIG/GGG (111) film analyzed from 20° to 90°. (c) Temperature dependence of M_s for the GdIG (150 nm)/GGG (111) film. Red line is the fitting curve and the inset picture is a sketch of three different magnetic sub-lattices of GdIG. Double-headed arrows indicate exchange interactions. Inset figure shows the hysteresis loops of the GdIG (150 nm)/GGG (111) film measured at 70 K, 190 K, and 280 K.

3. Results and discussion

The Fe^{3+} ions in a unit cell of GdIG are surrounded by 8 oxygen octahedrons (a sites) and 12 oxygen tetrahedrons (d sites). The Gd^{3+} ions sit in 12 oxygen dodecahedrons (c sites). The interaction between the a-site Fe^{3+} ions and the d-site Fe^{3+} ions is an anti-ferromagnetic super-exchange (exchange constant J_{ad}) interaction, resulting in a net magnetic moment M_{Fe} because of the unequal numbers of the a-site and d-site Fe^{3+} ions. The Gd^{3+} ions are ferromagnetically and anti-ferromagnetically coupled to the a-site Fe^{3+} ions (exchange constant J_{ac}) and the d-site Fe^{3+} ions (exchange con-

stant J_{dc}), respectively,[29,30] as schematically shown in the inset of Fig. 1(c). The magnetic moment of the Gd^{3+} ions M_{Gd} is anti-parallel to M_{Fe} because of $|J_{ac}| \ll |J_{dc}|$.[31,32] Owing to the negligible interaction between the Gd^{3+} ions and $|J_{dc}| \ll |J_{ad}|$, M_{Gd} declines more rapidly than M_{Fe} with increasing temperature. Eventually, M_{Gd} and M_{Fe} cancel out each other at T_M to give the total magnetic moment of zero.[33] Figure 1(c) displays the T-dependence of the saturation magnetization M_s of our GdIG (150 nm)/GGG (111) sample, where M_s is extracted from the hysteresis loops. The hysteresis loops measured at three typical temperatures are shown in the inset of Fig. 1(c). The coercivity is small, indicating a small anisotropy of GdIG.[34] It is observed that the behavior of M_s is consistent with the above description and T_M is ~ 185 K for this sample. This value is lower than the bulk value for GdIG ~ 288 K,[31] which may be due to the strain effect of the GGG substrate on the PLD grown film.[35]

In order to estimate the strength of the exchange interactions in the GdIG film, we fitted the curve of M_s as a function of T [Fig. 1(c)], with Néel's theory on ferrimagnetism. Because J_{ad} is much larger than all other exchange constants, the a-site and d-site Fe sub-lattices are treated as a single entity with a net magnetic moment. Thus, GdIG can be simplified as a two-sub-lattice ferrimagnet including the Fe and Gd sub-lattices. According to the molecular field approximation, the T-dependence of Fe and Gd sub-lattice moments can be obtained by[36,37]

$$M_{Fe(Gd)}(T) = M_{Fe(Gd)}(0) B_J(x_{Fe(Gd)}), \tag{1}$$

with

$$x_{Fe} = g_{Fe} J_{Fe} \mu_B (\mu_0 \boldsymbol{H} + N_{dd} \boldsymbol{M}_{Fe} + N_{dc} \boldsymbol{M}_{Gd}) / (k_B T),$$
$$x_{Gd} = g_{Gd} J_{Gd} \mu_B (\mu_0 \boldsymbol{H} + N_{dc} \boldsymbol{M}_{Fe}) / (k_B T),$$

where $g_{Fe(Gd)} = 2$ is the Landé factor of Fe^{3+} (Gd^{3+}),[38,39] $J_{Fe} = 5/2$ and $J_{Gd} = 7/2$ are the angular momentum quantum numbers of the Fe^{3+} and Gd^{3+} ions, respectively; B_J is the Brillouin function; μ_B is the Bohr magneton; μ_0 is the vacuum permeability; N_{dd} is the intra-sub-lattice molecular field constant between the Fe^{3+} ions; N_{dc} is the inter-sub-lattice molecular field constant; and k_B is the Boltzmann constant. Here, the interaction between Gd^{3+} ions is ignored. With the Curie temperature $T_c \sim 550$ K[29] and $\boldsymbol{H} = 0$, we used the expression $M_s = ||M_{Fe}| - |M_{Gd}||$ and Eq. (1) to evaluate the goodness of fit. The equations fits very well with the data, as shown by the red line in Fig. 1(c), with $N_{dd} = 68.6\ \mathrm{T}/\mu_B$ and $N_{dc} = 4.4\ \mathrm{T}/\mu_B$, which correspond to the molecular fields of ~ 332 T between a- sites and d-sites Fe^{3+} ions and ~ 21 T (for Gd) between Fe^{3+} and Gd^{3+} ions around T_M, respectively.[36,40] The yielded $T_M = 183$ K is close to the experimental value. Such good agreement indicates that the molecular field approximation can accurately describe the evolution of the sub-lattice magnetic moments of the Fe^{3+} and Gd^{3+} ions as functions of T and H.

In normal metal/ferromagnetic insulator bilayers, the longitudinal resistivity (ρ) of the normal metal depends on the orientation of the magnetic moment, which is the SMR.[22,28] Considering ferrimagnetism with two magnetic sub-lattices, both sub-lattices contribute to the SMR. ρ is then given by[25,41]

$$\rho = \rho_0 - \Delta\rho_1 \cos^2\varphi_1 - \Delta\rho_2 \cos^2\varphi_2, \tag{2}$$

where φ_1 (φ_2) is the angle between the magnetic moment $\boldsymbol{M}_1$ ($\boldsymbol{M}_2$) of the sub-lattice and the spin polarization (σ) of the spin-Hall-generated spin current, $\Delta\rho_1$ ($\Delta\rho_2$) is the corresponding SMR coefficient of the magnetic sub-lattice, and ρ_0 is a constant resistivity offset. For an anti-ferromagnet or a ferromagnet close to T_M, the Néel vector is defined as $\boldsymbol{n} = (\boldsymbol{M}_1 - \boldsymbol{M}_2)/|\boldsymbol{M}_1 - \boldsymbol{M}_2|$. When $\boldsymbol{M}_1 = -\boldsymbol{M}_2$, one obtains $\rho = \rho_0 - (\Delta\rho_1 + \Delta\rho_2)\cos^2\varphi_n$, where φ_n is the angle between $\boldsymbol{n}$ and σ, which is the same as the expression for the ferromagnet. Therefore, one can determine the direction of $\boldsymbol{n}$ using ρ.

The experimental geometry for the MR measurements is schematically shown in Fig. 2(a). The directions of the DC and the normal direction to the sample are defined as the x and z directions, respectively. The resistivities of the 3-nm thick Pt strip on GdIG (150 nm) film were measured at 300 K by applying $\boldsymbol{H}$ along the x, y, and z axes, respectively. ρ significantly depends on the direction of $\boldsymbol{H}$, and consequently the magnetization $\boldsymbol{M}$, as shown in Fig. 2(b). ρ increases with increasing H after M is saturated. This behavior was previously attributed to the Hanle MR[42] and the "new MR".[43] More importantly, at high field, the expression $\rho_{\parallel} \approx \rho_{\perp} > \rho_T$ still holds and the MR ratios $\Delta\rho_{\parallel}/\rho_T = (\rho_{\parallel} - \rho_T)/\rho_T$ and $\Delta\rho_{\perp}/\rho_T = (\rho_{\perp} - \rho_T)/\rho_T$, remain positive, where $\rho_{\parallel}$, ρ_T and $\rho_{\perp}$ are the resistivities for $\boldsymbol{H} \parallel x$, $\boldsymbol{H} \parallel y$, and $\boldsymbol{H} \parallel z$, respectively. Angular-dependent MR (ADMR) measurements were then performed in a constant applied field while rotating the samples. The results for $\mu_0 H = 1$ T are shown in Fig. 2(c), where $\Delta\rho/\rho(\mathrm{angle}) = [\rho(\mathrm{angle}) - \rho(\mathrm{angle} = 90^\circ)]/\rho(\mathrm{angle} = 90^\circ)$, and the angles α, β, and γ are defined in Fig. 2(a). $\Delta\rho/\rho(\alpha)$ and $\Delta\rho/\rho(\beta)$ are positive for all angles. For the α-scan, the field is large enough to achieve $\boldsymbol{H} \parallel \boldsymbol{M}$. $\Delta\rho/\rho(\alpha)$ is well fitted with the $\cos^2\alpha$ function. For the β-scan, $\Delta\rho/\rho(\beta)$ deviates from the $\cos^2\beta$ function owing to the misalignment of $\boldsymbol{H}$ and $\boldsymbol{M}$ caused by the demagnetization field.[44] The amplitude of the γ-scan is one order of magnitude smaller than those of the α- and β-scans. These features are similar to those of the $Pt/Y_3Fe_5O_{12}$ (YIG) system and are consistent with the

SMR mechanism.[24,25] As ρ measured with $\boldsymbol{H}$ swept along the x and z axes and the ADMR for the α- and the β-scans are almost identical after $\boldsymbol{M}$ is saturated, we focused on the measurement of $\boldsymbol{H}$ applied along the x and y axes and the α-scan in the following studies.

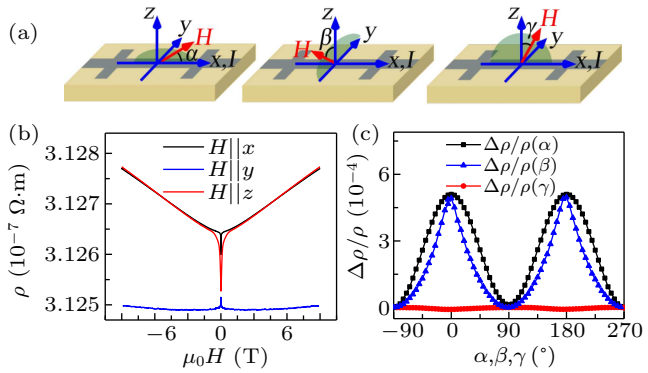


Fig. 2. (a) Schematic diagram of the MR measurements in three planes. Film plane is defined as the x–y plane. Current is applied along the x direction. α, β and γ are the angles between $\boldsymbol{H}$ and x (in x–y plane), z (in y–z plane), and z (in x–z plane) axes, respectively. (b) Resistivity as a function of field measured on the Pt (3 nm)/GdIG (150 nm)/GGG (111) sample for field applied along x, y, and z axes. (c) ADMRs measured in the x–y, y–z, and x–z planes with $\mu_0 H = 1$ T. All measurements are performed at 300 K.

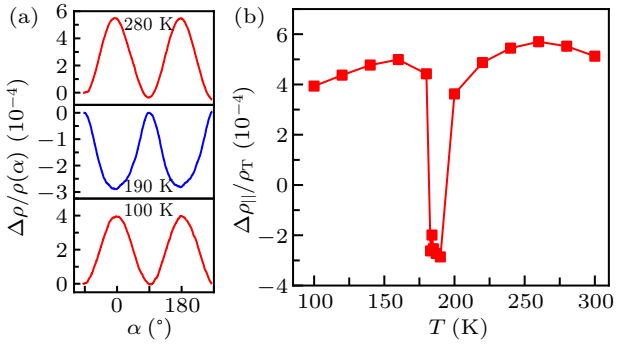


Fig. 3. (a) ADMRs measured in the x–y plane for the Pt (3 nm)/GdIG (150 nm)/GGG (111) sample at three different temperatures with $\mu_0 H = 1$ T. (b) Temperature-dependence of the SMR ratios extracted from the ADMRs measured in the x–y plane with $\mu_0 H = 1$ T.

Figure 3(a) shows the ADMR results of the α-scans at $\mu_0 H = 1$ T and three typical temperatures (100 K, 190 K, and 280 K). At $T = 280$ K and 100 K, which are far from T_{M}, $\Delta\rho/\rho(\alpha)$ is always positive, meaning that $\rho_{\parallel} > \rho_{\mathrm{T}}$. At $T = 190$ K, in the vicinity of T_{M}, the curve is shifted by 90° as compared to the data measured at $T = 280$ K and 100 K, leading to $\rho_{\parallel} < \rho_{\mathrm{T}}$ or a negative SMR. The ADMR at 190 K exhibits a slight deviation from the $\cos^2\alpha$ function because of the misalignment of $\boldsymbol{H}$ and $\boldsymbol{M}$ in the vicinity of T_{M}. The ADMR around T_{M} could produce complex angular dependence since sub-lattice magnetic moments have different angular dependence on magnetic field for an inhomogeneous sample.[20] We carried out the same measurements from $T = 300$ K to $T = 100$ K. The extracted SMR ratio is shown in Fig. 3(b). The SMR is negative close to T_{M} of GdIG. In comparison, for the ferrimagnetic insulator YIG, which has no magnetization compensation point, the SMR for Pt/YIG is positive,[46,47] suggesting that our observation is related to the magnetic structure transition for GdIG close to T_{M}.

A simple method to directly assess the magnetic structure transition is through magnetic moment measurement techniques such as SQUID-VSM. For our GdIG (150 nm)/GGG (0.5 mm) sample, the magnetic moment of the GGG substrate is approximately two and three orders of magnitude higher than that of the GdIG film at 300 K and 190 K, respectively, for $\mu_0 H = 1$ T. Therefore, this approach is not suitable because the paramagnetic signal of the GGG substrate is too large to accurately determine the magnetic structure transition of GdIG. Instead, we performed MR measurements as a function of H to investigate the negative MR close to T_{M}. This method has been verified to be a reliable tool in determining the orientation of the Néel vector of an anti-ferromagnetic insulator.[24–26] Figure 4(a) shows $\rho_{\parallel}$ and ρ_{T} as a function of H for H applied along the x and y axes, respectively, at 190 K. The sharp downward peak of $\rho_{\parallel}$ near $H = 0$ is due to the magnetization reversal at the coercivity of GdIG, similar to the peaks in Fig. 2(b). After H exceeds the saturation field (~ 0.1 T), $\boldsymbol{M}$ should be aligned with $\boldsymbol{H}$. In this range of magnetic field, the SMR predicts the constant $\rho_{\parallel}$ and ρ_{T}, and the "new MR" mechanism predicts the monotonic increases in $\rho_{\parallel}$ and ρ_{T}. However, our observations are inconsistent with these two predictions. $\rho_{\parallel}$ and ρ_{T} notably demonstrate non-monotonic behaviors with minimum and maximum values, respectively, as shown in Fig. 4(a). As a result, $\Delta\rho_{\parallel}/\rho_{\mathrm{T}}$ is positive in low magnetic fields, negative in the field range of ~ 0.40 T$< \mu_0 H <\sim 1.65$ T with a maximum negative SMR ratio of approximately -3.2×10^{-4} at ~ 0.8 T, and then turns positive at $\mu_0 H >\sim 1.65$ T, as shown in Fig. 4(b).

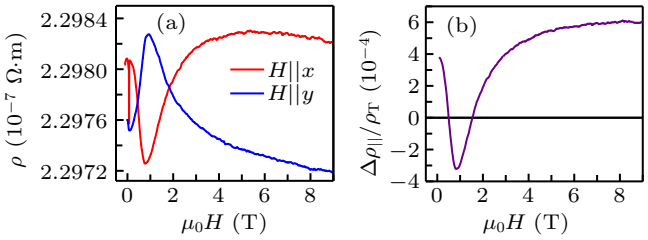


Fig. 4. (a) Resistivity as a function of H with H applied along the x and y axes at 190 K. (b) Calculated $\Delta\rho_{\parallel}/\rho_{\mathrm{T}}$ from 0.1 T to 9 T using the data from (a).

These findings are only observed when T is close to T_{M} strongly suggesting that this phenomenon is connected with the compensated ferrimagnetism. A negative SMR was observed in Pt/NiO/YIG tri-layers due to a critical temperature where the SMR changed from positive to negative with decreasing T.[26,48–50] The negative SMR is attributed to either the occurrence of spin-flip scattering for the reflected spin at the NiO/YIG interface or the spin being reflected back at the Pt/NiO interface and the SF coupling between YIG and NiO. Whichever conclusion is correct, neither can be

applied to our system because of the absence of the anti-ferromagnet/ferromagnet interface for the spin-flipping scattering or SF coupling in a single GdIG layer. A negative SMR was also reported in the heterostructure of a heavy metal Pt and an anti-ferromagnet,[24] which is explained by the 90° phase-shift due to the H-induced SF. However, the SMR does not change sign in presence of sweeping H, implying that the explanation of a negative SMR cannot be applied to our system. In fact, a negative SMR was previously observed in Pt and indium/yttrium-doped GdIG ($Y_1Gd_2Fe_4In_1O_{12}$) bi-layers close to the T_M, which is attributed to the negligible contribution of Gd to the SMR and $\boldsymbol{M}_{Fe}$ perpendicular to $\boldsymbol{H}$ at a relatively large $\boldsymbol{H}$ close to T_M.[41] The second change in the sign of SMR can occur when $\boldsymbol{H}$ exceeds the AFM coupling strength ($\sim$ 21 T for our sample according to the fitting results with Eq. (1)) to align $\boldsymbol{M}_{Gd}$ and $\boldsymbol{M}_{Fe}$ to a parallel position.[36,41] However, this is inconsistent with our observation that the second change in the sign of SMR occurs at $\mu_0 H < 2$ T. Therefore, the conclusion that the second SMR sign change is due to the alignment of $\boldsymbol{M}_{Gd}$ and $\boldsymbol{M}_{Fe}$ is invalidated.

Here, we proposed a model within the molecular field approximation framework that fits our observations. The energy E in GdIG due to the Zeeman energy of the molecular fields and the external field is given by

$$E(\theta_{Fe}, \theta_{Gd}) = 2N_{dc}\boldsymbol{M}_{Fe}\cdot\boldsymbol{M}_{Gd} - \mu_0\boldsymbol{H}\cdot\boldsymbol{M}_{Fe} - \mu_0\boldsymbol{H}\cdot\boldsymbol{M}_{Gd}, \quad (3)$$

where $\theta_{Fe(Gd)}$ is the angle between $\boldsymbol{M}_{Fe(Gd)}$ and $\boldsymbol{H}$, as defined in the inset of Fig. 5(a). Because of the small anisotropy of the (111)-oriented GdIG,[34] the magneto-crystalline anisotropy energy is ignored. Combining Eqs. (1) and (3), the H-dependences of θ_{Fe} and θ_{Gd} can be calculated numerically by computing the minimum value of $E(\theta_{Fe}, \theta_{Gd})$. The result at $T = 190$ K is shown in Fig. 5(a). At low magnetic fields, the normalized Néel vector $\boldsymbol{n}_{GdIG} = (\boldsymbol{M}_{Fe} - \boldsymbol{M}_{Gd})/|\boldsymbol{M}_{Fe} - \boldsymbol{M}_{Gd}|$ is parallel to $\boldsymbol{H}$ due to the small net magnetic moment. At $\mu_0 H \approx 0.9$ T, an SF transition, that is $\boldsymbol{n}_{GdIG} \perp \boldsymbol{H}$, occurs. However, with a further increase in the magnetic field, unlike antiferromagnets in which both sub-lattice moments tilt towards $\boldsymbol{H}$, $\boldsymbol{M}_{Fe}$, and $\boldsymbol{M}_{Gd}$ tend to align antiparallel and parallel with $\boldsymbol{H}$, respectively, and $\boldsymbol{n}_{GdIG}$ aligns anti-parallel with $\boldsymbol{H}$. The bi-reorientation transition of the Néel vector is shown in Fig. 5(b). With $\theta_{Fe}(H)$ and the SMR mainly contributed by the Fe sub-lattice moments suggested by Ref. [41], ρ is calculated from Eq. (2) as

$$\begin{aligned} \rho_{\parallel} &= \rho_0 + \Delta\rho_{Fe}\cos^2\theta_{Fe}(H), \\ \rho_T &= \rho_0 + \Delta\rho_{Fe}\sin^2\theta_{Fe}(H), \end{aligned} \quad (4)$$

where $\Delta\rho_{Fe}$ is the SMR coefficient for the Fe sub-lattice. The calculated results of Eq. (4), as shown in Fig. 5(c), are in good agreement with the experimental results [as shown in Fig. 4(a)]. Based on the good agreement between the theoretical and the experimental results, we concluded that the observed SMR behaviors originate from the field-induced Néel-vector bi-reorientation.

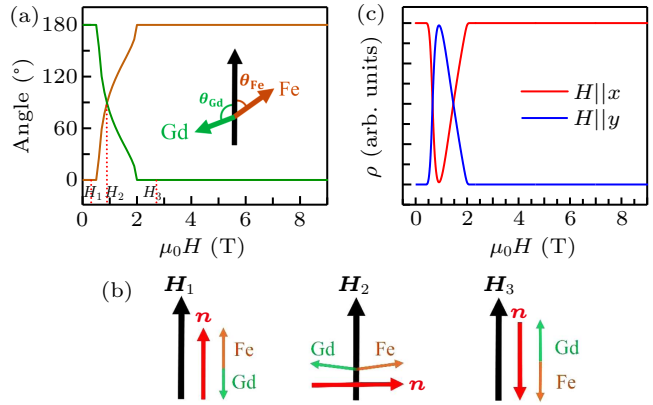


Fig. 5. (a) Calculated results of θ_{Fe} (brown line) and θ_{Gd} (green line) using Eqs. (1) and (3) at 190 K and the inset defines θ_{Fe} and θ_{Gd}. (b) Orientations of the Fe sub-lattice and Gd sub-lattice moments with respect to the $\boldsymbol{H}$ where $\boldsymbol{H} = H_1$, H_2, and H_3, which are defined in (a), $\boldsymbol{n}$ is the Néel vector of GdIG. (c) Calculated resistivity as a function of field using Eq. (4) and the data shown in (a).

In addition to theoretical calculations, this observation can be understood phenomenologically. Because of the very strong interaction between the Fe^{3+} ions and the weak interaction between the Gd^{3+} ions, the Fe and Gd sub-lattices in GdIG can be considered individually as a "ferromagnetic system" and a "paramagnetic system", respectively. M_{Gd} is induced by the external and molecular fields. At $T \sim T_M$, that is, $M_{Fe} \approx -M_{Gd}$, GdIG undergoes an SF transition or a reorientation of $\boldsymbol{n}_{GdIG}$ for a relatively large magnetic field similar to an anti-ferromagnet. On further increasing the magnetic field, M_{Fe} remains constant as a "ferromagnet". In contrast, M_{Gd} increases significantly as a "paramagnet" when the magnetic field is increased leading to $|M_{Fe}| < |M_{Gd}|$ or the transformation from an anti-ferromagnet into a ferrimagnet. As a result, $\boldsymbol{M}_{Fe}$ or $\boldsymbol{n}_{GdIG}$ is aligned antiparallel with $\boldsymbol{H}$ above a critical magnetic field, indicating the occurrence of a second re-orientation [Fig. 5(b)]. Our findings indicate that the direction of the Néel vector of a ferrimagnet can be tuned across a wide range from 0° to 90° and then to 180° by the appropriate external magnetic field close to the T_M.

4. Conclusions

We systematically investigated SMR in Pt/GdIG bilayers under a wide range of temperatures and magnetic fields. Our findings indicate that SMR in Pt/GdIG bilayers is positive for temperatures far from T_M, similar to that of the Pt/YIG bilayer. In the vicinity of T_M, the field-dependent SMR ratio not only exhibits a non-monotonic behavior, but also changes its sign twice. We attribute this behavior to the field-induced Néel

vector bi-reorientation. This observation can be explained by the fact that the Gd sub-lattice moment increases more rapidly than the Fe sub-lattice moment by the external field since the molecular field of the Gd ions are much weaker than that of the Fe ions. We also showed that the calculations based on the molecular field approximation and SMR theory can accurately predict the experimental phenomena. Our results demonstrate that SMR is a simple method for detecting accurately the Néel vector of a ferrimagnet. The direction of the Néel vector of a ferrimagnet can be tuned across a wide range by an external magnetic field in the vicinity of T_{M}.

References

[1] Ivanov B A 2019 *Low Temp. Phys.* **45** 935
[2] Caretta L, Mann M, Büttner F, Ueda K, Pfau B, Günther C M, Hessing P, Churikova A, Klose C, Schneider M, Engel D, Marcus C, Bono D, Bagschik K, Eisebitt S and Beach G S D 2018 *Nat. Nanotechnol.* **13** 1154
[3] Yang S H, Ryu K S and Parkin S 2015 *Nat. Nanotechnol.* **10** 221
[4] Mishra R, Yu J, Qiu X, Motapothula M, Venkatesan T and Yang H 2017 *Phys. Rev. Lett.* **118** 167201
[5] Kim K J, Kim S K, Hirata Y, Oh S H, Tono T, Kim D H, Okuno T, Ham W S, Kim S, Go G, Tserkovnyak Y, Tsukamoto A, Moriyama T, Lee K J and Ono T 2017 *Nat. Mater.* **16** 1187
[6] Baltz V, Manchon A, Tsoi M, Moriyama T, Ono T and Tserkovnyak Y 2018 *Rev. Mod. Phys.* **90** 15005
[7] Wadley P, Howells B, Elezny J, Andrews C, Hills V, Campion R P, Novak V, Olejnik K, Maccherozzi F, Dhesi S S, Martin S Y, Wagner T, Wunderlich J, Freimuth F, Mokrousov Y, Kune J, Chauhan J S, Grzybowski M J, Rushforth A W, Edmonds K W, Gallagher B L and Jungwirth T 2016 *Science* **351** 587
[8] Chen X Z, Zarzuela R, Zhang J, Song C, Zhou X F, Shi G Y, Li F, Zhou H A, Jiang W J, Pan F and Tserkovnyak Y 2018 *Phys. Rev. Lett.* **120** 207204
[9] Baldrati L, Gomonay O, Ross A, Filianina M, Lebrun R, Ramos R, Leveille C, Fuhrmann F, Forrest T R, Maccherozzi F, Valencia S, Kronast F, Saitoh E, Sinova J and Kläui M 2019 *Phys. Rev. Lett.* **123** 177201
[10] Chiang C C, Huang S Y, Qu D, Wu P H and Chien C L 2019 *Phys. Rev. Lett.* **123** 227203
[11] Mills D L 1968 *Phys. Rev. Lett.* **20** 18
[12] Wu S M, Zhang W, KC A, Borisov P, Pearson J E, Jiang J S, Lederman D, Hoffmann A and Bhattacharya A 2016 *Phys. Rev. Lett.* **116** 097204
[13] Lebrun R, Ross A, Bender S A, Qaiumzadeh A, Baldrati L, Cramer J, Brataas A, Duine R A and Kläui M 2018 *Nature* **561** 222
[14] Qaiumzadeh A, Skarsvåg H, Holmqvist C and Brataas A 2017 *Phys. Rev. Lett.* **118** 137201
[15] Yuan W, Zhu Q, Su T, Yao Y, Xing W, Chen Y, Ma Y, Lin X, Shi J, Shindou R, Xie X C and Han W 2018 *Sci. Adv.* **4** eaat1098
[16] Jacobs I S 1961 *J. Appl. Phys.* **32** S61
[17] Machado F L A, Ribeiro P R T, Holanda J, Rodríguez-Suárez R L, Azevedo A and Rezende S M 2017 *Phys. Rev. B* **95** 104418
[18] Strohm C, Roth T, Detlefs C, van der Linden P and Mathon O 2012 *Phys. Rev. B* **86** 214421
[19] Becker J, Tsukamoto A, Kirilyuk A, Maan J C, Rasing T, Christianen P C M and Kimel A V 2017 *Phys. Rev. Lett.* **118** 117203
[20] Dong B W, Cramer J, Ganzhorn K, Yuan H Y, Guo E J, Goennenwein S T B and Kläui M 2017 *J. Phys.: Condens. Matter* **30** 035802
[21] Bernasconi J and Kuse D 1971 *Phys. Rev. B* **3** 811
[22] Nakayama H, Althammer M, Chen Y T, Uchida K, Kajiwara Y, Kikuchi D, Ohtani T, Geprägs S, Opel M, Takahashi S, Gross R, Bauer G E W, Goennenwein S T B and Saitoh E 2013 *Phys. Rev. Lett.* **110** 206601
[23] Wang S, Li G, Wang J, Tian Y, Zhang H, Zou L, Sun J and Jin K 2018 *Chin. Phys. B* **27** 117201
[24] Hoogeboom G R, Aqeel A, Kuschel T, Palstra T T M and Van Wees B J 2017 *Appl. Phys. Lett.* **111** 052409
[25] Fischer J, Gomonay O, Schlitz R, Ganzhorn K, Vlietstra N, Althammer M, Huebl H, Opel M, Gross R, Goennenwein S T B and Geprägs S 2018 *Phys. Rev. B* **97** 014417
[26] Hou D, Qiu Z, Barker J, Sato K, Yamamoto K, Vélez S, Gomez-Perez J M, Hueso L E, Casanova F and Saitoh E 2017 *Phys. Rev. Lett.* **118** 147202
[27] Smart J S 1955 *Am. J. Phys.* **23** 356
[28] Chen Y T, Takahashi S, Nakayama H, Althammer M, Goennenwein S T B, Saitoh E and Bauer G E W 2013 *Phys. Rev. B* **87** 144411
[29] Bayaraa T, Xu C, Campbell D and Bellaiche L 2019 *Phys. Rev. B* **100** 214412
[30] Wang L W, Xie L S, Xu P X and Xia K 2020 *Phys. Rev. B* **101** 165137
[31] Rodić D, Tomkowicz Z, Novaković L, Szytula A and Napijalo M L 1990 *Solid State Commun.* **73** 243
[32] Rovani P R, Ferreira A S, Pereira A S and de Lima J C 2017 *J. Appl. Phys.* **122** 035904
[33] Aliev S M, Kamilov I K, Aliev M S and Ibaev Z G 2014 *Phys. Solid State* **56** 1114
[34] Mee C D 1967 *Contemp. Phys.* **8** 385
[35] Sawatzky E and Kay E 1969 *J. Appl. Phys.* **40** 1460
[36] Clark A E and Callen E 1968 *J. Appl. Phys.* **39** 5972
[37] Anderson P W 1950 *Phys. Rev.* **79** 705
[38] Nibarger J P, Lopusnik R, Celinski Z and Silva T J 2003 *Appl. Phys. Lett.* **83** 93
[39] Hellman F, Queen D R, Potok R M and Zink B L 2000 *Phys. Rev. Lett.* **84** 5411
[40] Eremenko V V and Kharchenko N F 1979 *Phase Transitions* **1** 61
[41] Ganzhorn K, Barker J, Schlitz R, Piot B A, Ollefs K, Guillou F, Wilhelm F, Rogalev A, Opel M, Althammer M, Geprägs S, Huebl H, Gross R, Bauer G E W and Goennenwein S T B 2016 *Phys. Rev. B* **94** 094401
[42] Velez S, Golovach V N, Bedoya-Pinto A, Isasa M, Sagasta E, Abadia M, Rogero C, Hueso L E, Bergeret F S and Casanova F 2016 *Phys. Rev. Lett.* **116** 016603
[43] Miao B F, Huang S Y, Qu D and Chien C L 2014 *Phys. Rev. Lett.* **112** 236601
[44] Wang P, Jiang S W, Luan Z Z, Zhou L F, Ding H F, Zhou Y, Tao X D and Wu D 2016 *Appl. Phys. Lett.* **109** 112406
[45] Luan Z Z, Zhou L F, Wang P, Zhang S, Du J, Xiao J, Liu R H and Wu D 2019 *Phys. Rev. B* **99** 174406
[46] Marmion S R, Ali M, McLaren M, Williams D A and Hickey B J 2014 *Phys. Rev. B* **89** 220404
[47] Wang S, Zou L, Zhang X, Cai J, Wang S, Shen B and Sun J 2015 *Nanoscale* **7** 17812
[48] Lin W and Chien C L 2017 *Phys. Rev. Lett.* **118** 067202
[49] Shang T, Zhan Q F, Yang H L, Zuo Z H, Xie Y L, Liu L P, Zhang S L, Zhang Y, Li H H, Wang B M, Wu Y H, Zhang S and Li R W 2016 *Appl. Phys. Lett.* **109** 032410
[50] Luan Z Z, Chang F F, Wang P, Zhou L F, Cooper J F K, Kinane C J, Langridge S, Cai J W, Du J, Zhu T and Wu D 2018 *Appl. Phys. Lett.* **113** 072406